Evaluation of Underlying Causative Factors for Earthquake-Induced Landslides and Landslide Susceptibility Mapping in Upper Indrawati Watershed, Nepal

Pawan Gautam (pawan.gtm@gmail.com)
Kyushu University https://orcid.org/0000-0002-7918-314X

Tetsuya Kubota
Kyushu University Faculty of Agriculture Graduate School of Bioresource and Bioenvironmental Sciences: Kyushu Daigaku Nogakubu Daigakuin Seibutsu Shigen Kankyo Kagakufu

Aril Aditian
The AHA Centre, East Jakarta

Research

Keywords: Earthquake-induced Landslide, Landslide Distribution, Landslide Susceptibility Mapping, Logistic Regression, Upper-Indrawati Watershed

Posted Date: October 5th, 2020

DOI: https://doi.org/10.21203/rs.3.rs-72223/v1

Abstract

The main objectives of this study are to assess the underlying causative factors for landslide occurrence due to earthquake in upper Indrawati Watershed of Nepal and evaluating the region prone to landslide using Landslide Susceptibility Mapping (LSM). We used logistic regression (LR) for LSM on geographic information system (GIS) platform. Nine causal factors (CF) including slope angle, aspect, elevation, curvature, distance to fault and river, geological formation, seismic intensity, and land cover were considered for LSM. We assessed the distribution of landslide among the classes of each CF to understand the relationship of CF and landslides. The northern part of the study area, which is dominated by steep rocky slope have a higher distribution of earthquake-induced landslides. Among the CF, 'slope' showed the positive correlation as landslide distribution is increasing with increasing slope. However, LR analysis depict 'distance to the fault' is the best predictor with the highest coefficient value. Susceptibility map was validated by assessing the correctly classified landslides under susceptibility categories, generated in five discrete classes using natural break (Jenk) methods. Calculation of area under curve (AUC) and seed cell area index (SCAI) were performed to validate the susceptibility map. The LSM approach shows good accuracy with respective AUC value for success rate and prediction rate of 0.795 and 0.702. Similarly, the decreasing SCAI value from very low to very high susceptibility categories advise satisfactory accuracy of LSM approach.

Background And Introduction

Landslides, either triggered by an earthquake or rainfall (Garcia-Rodriguez et al., 2008), pose costly and deadly threats to the mountainous country (Nowicki et al., 2014; Robinson et al., 2017). It subsequently damages the houses and basic infrastructures, economics, and human prosperity (Corominas et al., 2014) and considered as vital geological hazards in the high mountain region (Nefeslioglu, 2008). Earthquake alone triggers a lot of landslides (Xu and Xu, 2012; Xu et al., 2013a) in the mountainous region (Kamp et al., 2008) consequently remarked as subordinate hazards of earthquake (Keefer, 1994, 2002; Li et. al., 2014). Notably, the 25 April 2015 Gorkha earthquake of Nepal and its aftershock not only responsible for deaths of nine thousand people and economic losses of billions US dollars (GoN, 2015), but also triggered more than 25,000 landslides (Roback et al., 2018), which included small-scale rock falls to valley blocking landslides in several areas (Kargel et al., 2016). The landslides obstructed the accessibility to earthquake-affected area hindering the post-earthquake relief activities (Kargel et al., 2016) multiplying the effects of the earthquake.

Despite, earthquake, an external factor, triggered many landslides (Pourghasemi and Rahmati, 2018), several conditioning factors are responsible for occurrences of landslides including topography, geology, and environmental parameters (Suzen and Kayo, 2012). Anthropogenic interactions including rapid infrastructure development (Petley et al., 2007) if combine with ground shaking become a major triggering factor for landslide occurrences (Suzen and Kaya, 2011) in mountanous region (Robinson et al., 2017). Hence, it is necessary to identify the landslide distribution following an earthquake to understand the total impacts of the earthquake (Marzorati et al., 2002); Robinson and Davies, 2013).

Landslide susceptibility mapping (LSM) identifies landslide sensitive area considering the relationship between causal factors and past landslide (Fell et al., 2008) is key step for landslide monitoring and mitigation (Pourghasemi and Rahmati, 2018). Further, LSM is important for safe planning, disaster management, and future planning of earthquake stuck area (Xu et al., 2013a).

Many of the developed countries have adopted few technologies to understand the landslide risk of the earthquake which has been lacking in the Nepalese context. Despite several studies have been conducted regarding the landslides and its distribution after earthquake (e.g., Collins and Jibson, 2015; Goda et al., 2015; Gallen et al., 2016; Kargel et al., 2016; Robinson et al., 2017; Roback et al., 2018), there is still a gap in research regarding landslides and its damages due to the earthquakes (Kamp et al., 2008) mostly in developing countries including Nepal. As there is no agreed criteria for the selection of training and validation landslides (Xu et al., 2013b), most of the researcher employed random selection approach for susceptibility mapping (e.g., Ayalew and Yamagishi, 2005; Mancini et al., 2010; Chen et al., 2016; Aditian et al., 2018; Pourghasemi and Rahmati, 2018; Huang and Zhao, 2018). Significant to other studies, this study evaluates the susceptibility map using the validating dataset from another part within the study area among the different methods suggested by Remondo et el. (2003).

Multiple approaches have been adopted for LSM (Corominas et al., 2014) including heuristic approach (e.g., van Westen et al., 1999; Yalcin and Bulut, 2007; Kouli et al., 2010), statistical approach (e.g. Ayalew and Yamagishi, 2005; Kamp et al., 2008; Bai et al., 2010; Mancini et al., 2010; Xu et al., 2013a,b), and deterministic approach (e.g. Zhou et al., 2003). Broadly, it can be classified as qualitative and quantitative approaches (Ayalew and Yamagishi, 2005; Garcia-Rodriguez et al., 2008; Corominas et al., 2014). In the heuristic analysis, the weight assignment is based on the expert opinion (Fell et al., 2008; Xu et al., 2013b; Corominas et al., 2014) as a qualitative approach (Ayalew and Yamagishi, 2005). Both deterministic and statistical methods are a quantitative approach and are based on numerical expression of causal factors and landslides (Garcia-Rodriguez et al., 2008). The statistical method is based on the quantitative analysis of relationships between causal factors and landslide events (Ayalew and Yamagishi, 2005; Fell et al., 2008).

Several statistical approaches including bivariate probabilistic (e.g. Magliulo et al., 2008; Yilmaz, 2009), multivariate as logistic regression (LR; e.g. Dai and Lee, 2003; Ayalew and Yamagishi, 2005; Lee and Pradhan, 2007; Garcia-Rodriguez et al., 2008; Kamp et al., 2008; Bai et al., 2010; Mancini et al., 2010; Pradhan and Lee, 2010; Xu et al., 2013a; Aditian et al., 2018), artificial neural network (ANN; e.g. Nefeslioglu et al., 2008; Yilmaz, 2009; Pradhan and Lee, 2010; Bui et al., 2012; Aditian et al., 2018), and support vector machine (SVM; e.g. Yao et al., 2008; Xu et al., 2012) are commonly used for LSM. However, the consensus regarding best suiting methods for mapping has yet to be made (Garcia-Rodriguez et al., 2008; Corominas et al., 2014). Among them, LR can define the multivariate relationship of causal factors and landslides (Ayalew and Yamagishi, 2005; Lee and Pradhan, 2007) which logically can assign the weight depicting the most influencing causal factor as well as disregarding the less significant factors during the mapping process (Budimir et al., 2015). Hence, it produces more reliable results (Nandi and Shakoor, 2009). It is for that reason, LR approach is considered to be more suitable and is common in

LSM (Nandi and Shakoor, 2009; Budimir et al., 2015) especially in regional scale (e.g., Mancini et al., 2010; Pradhan and Lee, 2010; Xu et al., 2013a; Corominas et al., 2014).

In the wake of Gorkha earthquake, we studied the earthquake-induced landslides in Upper Indrawati Watershed of Nepal which is severely affected by the earthquake. The study area is in North of the small town called Melamchi (see in Fig. 2), where the effects due to the quake were reported severe in the study by Goda et al. (2016). Thus, our research aims to assess the impact of causal factors for the occurrence of landslides and susceptibility mapping to identify landslides sensitivity of the study area. We used descriptive statistics and logistic regression approaches integrating with Geographic Information System (GIS) for LSM (e.g., Garcia-Rodriguez et al., 2008; Kamp et al., 2008; Bai et al., 2010; Aditian et al., 2018). This study could also be replicated in another cathment area of high mountain region for susceptibility mapping.

Methods

Description of study area:

This research is conducted in Upper Indrawati Watershed (85^{o}33'N-85^{o}44'N; 27^{o}49'E-28^{o}07'E) of Sindhupalchok district, located in ~ 40 km north-east of Kathmandu, Nepal (Fig. 1: map of the study area with Fault line). We did not analyze the area with the altitude more than 4000 m because of the lack of geological data (no detailed data available in Department of Mines and Geology, Nepal), and unavailability of qualitative satellite images because of cloudy weather condition and snow-capped areas. Therefore, the altitude of the area we analyzed ranges from 796 m to 4000 m with the coverage of 364 km^{2} area. The slope gradient ranges from 0^{o} to 73^{o} with the mean slope of 31.6^{o}.

The study area belongs to higher Himalayan zone (Pre-Cambrian) geology dominated by Sermanthang formation and Dhad Khola gneiss formation covering 35% and 24% area respectively according to the data from Department of Mines and Geology, Nepal. Sermanthang formation mostly covers the high-altitude region of the study area which includes lithology of interbedded feldspathic schist, augen gneiss, quartzite, and biotic-feldspathic schist. However, Dhad Khola gneiss covers the lower altitudinal region including porphyroblastic gneiss, augen gneiss with a thin band of quartzite and schist, and migmatitic gneiss lithology. The study area also composed of main central thrust and two fault lines (southern edge and middle of the western boundary of the study area; Fig. 1).

The study area experienced many tremors after the Gorkha earthquake which originated in main Himalayan thrust followed by hundreds of aftershocks. These tremors increased the earthquake severity considerably in the study area (Goda et al., 2015) which amplified likely occurrences of landslides.

Landslide distribution:

Gorkha earthquake followed by hundreds of aftershocks (Parameswaran et al., 2015) triggered many landslides in the study area. We performed field observation, on-screen detection of an aerial

photographs, visual interpretation, and on screen as well as automatic detection of high-resolution satellite images following the Keefer et al. (2002) and Harp et al. (2011) for landslide detection (Xu et al., 2015). Use of high-resolution satellite image interpretation coupled with the field observation is quite useful and appropriate for coseismic landslides inventory (Xu et al., 2015). This is because the number, area, and volume of coseismic landslides is extensive (e.g., Keefer, 1994; Marc et al., 2016), and the location of landslides is spatially distributed over larger areas (Dai et al., 2011). Thus, we conducted onscreen digitization of post-earthquake high resolution, Geo Eye satellite imageries available on Google Earth in polygon format (Harp et al., 2011; Xu et al., 2014) and currently is appropriate alternative among the variety of methods available (Corominas et al., 2014). Even though its time consuming, it is more accurate than point based on susceptibility mapping (Xu et al., 2012). Furthermore, it was aided by field observation from Nov. 15 to Dec. 5, 2015.

Landslide distribution was expressed by landslide relative density (LRD) (Ayalew and Yamagishi, 2005), landslide number abundance (LNA) (Keefer, 2000; Xu et al., 2010; Xu et al., 2015) and landslide area abundance (LAA) (Dai et al., 2011; Xu et al., 2014; Xu et al., 2015) which helps to understand the effects of causal factors on landslide occurrences. LRD is the ratio of the frequency ratio value (FRV) of a class to total FRV of that causal factor and is calculated as suggested by Ayalew and Yamagishi (2005). LNA is the number of landslides per square kilometer, and LAA is the percentage of area affected by landslides (Xu et al., 2015).

Landslide causal factors:

The occurrence of the landslides depends upon the multiple causal factors. Even though seismic shaking is the driving force for the earthquake triggered landslides, local (natural and anthropogenic) factors play a dominant role (Kamp et al., 2008). Selection of the appropriate causal factors is essential for susceptibility mapping (Xu et al., 2013a). Casual factors should be measurable, varies spatially, available to cover the entire study area (Ayalew and Yamagishi, 2005) and have a certain degree of compatibility with the dependent variable (Garcia-Rodriguez et al., 2008). Hence, we selected nine factors for mapping which includes slope angle, aspect, elevation, curvature, distance to the fault and river, geological formation, seismic intensity, and land cover. The reason for the selection of causal factors is described in Table 1.

Table 1
Causal factors and its significance for landslide occurrence with the references

Causal Factors	Significance	Data Source
Slope Angle	Slope gradient, a predominant factor for mass wasting (Garcia-Rodriguez et al., 2008; Corominas et al., 2014). Steeper the slope gradient higher the chance of landslides (Kamp et al., 2008).	ASTER gDEM[1]
Aspect	Related to the weather condition, weathering and land cover thereby affect the occurrence of landslides (Garcia-Rodriguez et al., 2008, Kamp et al., 2008; Corominas et al., 2014).	ASTER gDEM
Elevation	Slope instability could be the result of changes in elevation (Corominas et al., 2014). The region having higher elevation mostly dominated by rocky slopes where the frequency of earthquake-induced landslides is higher (Owen et al., 2008).	ASTER gDEM
Curvature (total)	Curvature, a topographic factor, crucially important for rock fall and highly important for shallow landslides (Hasegawa et al., 2009; Corominas et al., 2014).	ASTER gDEM
Seismic intensity (PGA in %)	Earthquake shaking act as an additional driving force on the slope which favors the landslides (Duncan and Wright, 2005; Corominas et al., 2014): higher the energy of shaking, higher the risk of slope failure (Keefer, 2002; Delgado et al., 2011). We considered the peak ground acceleration (PGA) to understand the ground shaking.	USGS[2]
Geological formation	The strength and permeability of the slope depending on the lithology of the area thereby, is crucial conditioning factor for landslide occurrences (Dai and Lee, 2002; Corominas et al., 2014). We used geological formation according to the data availability as lithology varied according to the formation in the study area.	DMGN[3]
Distance to the fault	Distance to fault is highly relevant as both landslide conditioning and triggering factor (Corominas et al., 2014).	DMGN
Distance to the river	Landslide distribution is related to the distance to the river (Mancini et al., 2010; Corominas et al., 2014).	ASTER gDEM
Land cover	Mechanical anchoring of the land depends upon the land cover (Meusburger and Alewall, 2008) and is highly important conditioning factor for landslide occurrences (Montgomery et al., 2000; Garcia-Rodriguez et al., 2008; Corominas et al., 2014).	ICIMOD[4]

Note: [1]Advanced Spaceborne Thermal Emission and Reflection Radiometer (ASTER) global digital elevation model (gDEM), available on https://earthexplorer.usgs.gov; [2]United States Geological Survey (USGS), [3]Department of Mines and Geology, Nepal; [4]International Centre for Integrated Mountain Development (ICIMOD) (https://rds.icimod.org/Home/DataDetail?metadataId=9224)

All the causal factors were categorized from four to nine classes to understand their effect for landslide occurrences due to earthquake. Slope angle, elevation was classified using equal interval method in ArcGIS 10.3; natural break method was used for curvature to categorize continuous data in six discrete classes. We preserved the classes of the causal factor aspect (nine classes), seismic intensity (four

classes), geological formation (six classes) and land cover (seven classes). Buffering was performed in ArcGIS for distance to the fault (three km buffer provided seven classes) and distance to the river (four classes). The categorical map of the study area is presented in Fig. 2 (a-i).

The categorical factors (land cover, geological formation, and PGA) were dealt by creating dummy variables whereas the non-categorical factors with continuous data were dealt as they are (Nefeslioglu et al. 2008) for the purpose of susceptibility mapping using LR in this study. As the scales of the input variables (casual factors) are different, the input data was normalized from 0 and 1 in order to increase the speed and accuracy of data processing, using Eq. 1 following the study of Nefeslioglu et al. (2008).

$$X_{norm} = \frac{X_i - X_{min}}{X_{max} - X_{min}} \qquad (1)$$

where, X_{norm} is normalized value of X_i input data, X_i is the input data that should be normalized, X_{max} is the maximum value of the input data, and X_{min} is the minimum value of the input data.

Preparation of training and validation landslide:

All the inventoried landslides were divided as training landslide and validation landslide for LR modelling and LSM validating respectively (Aditian et al., 2018; Ba et al., 2018). As we only considered the earthquake induced landslide which were triggered by an event, the landslides of one part of the study area were used as the training landslide and another part as a validation landslide. We considered the Indrawati river (flowing from north to south) as the border: landslides occurred in the left bank of the river were used for LR modeling (training landslide) while landslides occurred in the right bank of the river were used for validation of the model (see Fig. 3).

In total, we mapped 402 earthquake-induced landslides in polygon format which covers 2.748 km^2. All the mapped landslides were rasterized in GIS platform in 30 × 30 m resolution for analysis, resembling the causal factors resolution as determined by digital elevation model (DEM), which covers a total of 3018 pixels. Out of which training landslide (left bank's landslides) consists of 309 landslide polygons with 2063 pixels whereas, validation landslide consists of 93 landslide polygons with 955 pixels. The equal number of non-landslides pixel for both training and validation landslide were selected for modelling and validating of LSM.

Landslide susceptibility mapping:

We used LR, a multivariate statistical approach for LSM in the study area (eg., Ayalew, and Yamagishi, 2005; Garcia-Rodriguez et al., 2008; Bai et al., 2010; Mancini et al., 2010; Xu et al., 2013a; Abedini et al., 2017; Aditian et al., 2018). LR is also called as a generalized linear model (GLM) for binary response variables (Hosmer and Lemeshow 2000). LR allows describing the effects of all the independent variables on dependent variables in the form of linear regression equation (Atkinson and Masari, 1998). LR has a distinct advantage in which the independent variables can be either continuous or (and) discrete

as if the link function is added to usual linear regression model (Bai et al., 2010), and not necessarily normally distributed (Garcia-Rodriguez, 2008; Bai et al., 2010). LR analysis is based on the analysis of dependency of a binary dependent variable having possible outcome of either 1 (landslide) or 0 (no landslide) to independent variables (landslide causal factors) (Mancini et al., 2010; Budimir et al., 2015). It calculates the probability of specific event occurrences, landslide occurrence in this case as in the study by Ayalew and Yamagishi (2005) which can be expressed as in Eq. (2).

$$P = 1/(1 + e^{-Z}) \qquad (2)$$

Where P is the probability of landslide occurrence, e is the exponential function and Z is the logit value which is expressed by a linear equation as;

$$Z = b_0 + b_1x_1 + b_2x_2 + \ldots\ldots + b_nx_n \qquad (3)$$

Where, b_0 is the intercept, b_1, b_2,……b_n are the coefficient of landslide causal factors x_1, x_2,……x_n respectively, n is the number of causal factors (9 in this study). The linear model is logistic regression and represents the presence and absence of landslides on independent variables (Bai et al., 2010).

The data were arranged in such a way that the scaled values of the causal factors were represented by the binary dependent variables (0 and 1), and LR was performed. The "glm" package in R 3.5.2 was used to perform GLM in the study area. Provided results were the coefficient of causal factors by the process of maximum likelihood criterion (Mancini et al., 2010).

Susceptibility scale of the region is relative (Fell et al., 2008) hence, obtained probability value were categorized in five discrete classes as susceptibility categories (extremely low, very low, low, medium and high) using the natural breaks (Jenks) method in ArcGIS (E.g., Lee and Sambath, 2006; Pradhan, 2010; Chalkias et al., 2014; and Aditian et al., 2018).

Map validation:

The overall performance of the mapping approach is assessed by identifying the correctly classified landslides under the susceptibility categories of LSM (Xu et al., 2013b). Area under the curve (AUC) was calculated to predict the accuracy of the model quantitatively (Akgun et al., 2012; Abedini et al., 2017; Ba et al., 2018). The AUC suggest the model's quality for reliable prediction of existence and non-existence of landslides (Aditian et al., 2018). The larger the AUC values, the higher the accuracy of model performance (Corominas et al., 2014). Additionally, the values close to 1.0 indicating perfect fit is the ideal condition whereas, close to 0.5 indicates the random fit (Carvalho et al., 2014).

We compared the LSM with both training and validation landslides. The curve obtained by overlaying susceptibility map with training landslide suggests the model's capability of classifying the area (Mancini

et al., 2010; Xu et al., 2012) and also called as success rate curve (Chung and Fabri, 2003; Aditian et al., 2018; Ba et al., 2018); and with validation landslide it is prediction rate curve (Lee and Pradhan 2007; Ba et al., 2018) suggesting the model's ability of landslide prediction (Chung and Fabri, 2003; Aditian et al., 2018). The AUC value generated from the success rate curves also indicates the correlation between dependent and independent variables in LR analysis (Mancini et al., 2010).

Further, the susceptibility map was validated using the seed cell area index (SCAI) as in Abedini et al. (2017), and Nicu and Asandulesei (2018) as suggested by Suzen and Doyuran (2004). The SCAI illustrates the landslide density on susceptibility class (Suzen and Doyuran, 2004) and is the ratio of the percentage of the area in susceptibility category to the percentage area of landslides occurred in that category (Abedini et al., 2017). The SCAI reflect the accuracy of the mapping approach qualitatively (Abedini et al., 2017). In ideal situation, the SCAI value is higher in low and very low susceptibility classes, whereas it is smaller in high and very high susceptibility classes (Kincal et al., 2009; Sdao et al., 2013; Chen et al., 2016; Abedini et al., 2017; Nicu and Asandulesei, 2018).

Results

Landslides distribution:

Landslides in the study area were distributed sparsely with the concentration in the Northern part of the study area (see landslide inventory in Fig. 4). The landslide frequency is higher in the northern part of the study area. This is because of the topology in northern region which is dominated by steeper slope and higher elevation. Most of the earthquake-induced landslides are rock and debris falls following the category of Varnes (1978) classification (Owen et al., 2008). We found an adequate number of rock-falls in the study area as the landslide concentration is higher in the northern part which is subjugated by the rocky slope. In this study, we did not include the debris flows, following the suggestion by Varnes (1978) as the mechanism of debris flows entirely different to other types of mass movement.

We assessed the concentration of earthquake-induced landslides in this study corresponding the study of Kargel et al. (2016). We categorized the area into eight categories considering the landslide number per km^2. As shown in Fig. 4, nearly 40% of the area is not affected by earthquake-induced landslides; with a frequency less than 0.5/km^2. Only 5% of the area had a landslide density (expressed regarding landslides #/km^2) of more than 40 (Fig. 4), suggesting the higher landslide zone. However, the area having landslides 10–20 per km^2 and 20–40 per km^2 covered the considerable area with 11% and 7% respectively.

The LRD, LNA, and LAA of the classes of causal factors are presented in Fig. 5 (a-i). LRD, LAA, and LNA are increased with slope angle reaching a maximum of 44%, 2.60% and 3.77/km^2 respectively (Fig. 5a). The LRD and LAA of southern aspect (southeast, south, and southwest) were higher with the value reaching maximum of 21% and 1.25% respectively. However, west and northwest aspect had higher LNA with the respective value of 8.54/km^2 and 3.46/km^2 (Fig. 5b).

The relationship of elevation and landslide frequency showed that the higher LRD (= 31%), LAA (= 1.15%) and LNA (= 1.66/km^2) were found in the elevation range (2400–3000) m and were decreased in either lesser or higher elevation classes (Fig. 5c). Both concave and convex curvature had higher landslide distribution with slightly more elevated in concave curvature reaching a maximum value of LRD (= 18%), LAA (= 1.64%) and LNA (= 2.38/km^2) in curvature class (= -22.89 to -4.75) (Fig. 5d).

In case of causal factor distance to the fault, class (6–9) km out of eight classes generated in ArcGIS with 3 km gradation from the fault line, have higher LRD, LAA and LNA with respective value of 36%, 1.4% and 2.03/km^2 with gradually decreasing on either side of the classes (Fig. 5e). Among the four classes of distance to the river, class (100–200) m have higher landslide distribution with the value of 38%, 1.11% and 1.61/km^2 for LRD, LAA and LNA respectively followed by the class (200–400) m (Fig. 5f).

Pangang formation of higher Himalayan zone (Pre-Cambrian) is available in the northernmost area of the watershed (Fig. 3 causal factors map), which has higher landslide distribution as LRD (= 41%), LAA (= 1.71%) and LNA (= 2.48/km^2) is higher followed by Sermanthang formation as shown in Fig. 5 g (also found in northern part). Hence, gneiss, schist and quartzite lithology of the higher Himalayan group were highly susceptible due to the earthquake-induced landslide in the study area.

As we were mapping seismic induced landslides susceptibility, we considered seismic intensity; which varied spatially throughout the study area, as a causal factor. LRD (= 43%), LAA (= 0.99%) and LNA (= 1.44/km^2) were found higher in the area which had low seismic intensity (20% peak ground acceleration, PGA) followed by the PGA class 50% (Fig. 5 h) among the four classes of PGA.

Landslide distribution in the open forest is higher in case of earthquake-induced landslides in the study area followed by shrubland reaching the maximum value of 31%, 1.16% and 1.69/km^2 for LRD, LAA and LNA respectively (Fig. 5i). Landslide frequency in the closed forest was also considerably higher compared to agricultural land in the study area. The reason behind this could be most of the forested area is distributed throughout the higher slope gradient as we overlaid the land cover class with slope gradient.

Landslide susceptibility modelling:

All the causal factors show the positive association for landslide occurrences in the study area except elevation, formation, and some classes of land cover (Table 2). We found the distance to the fault was the best predictor of landslide occurrences followed by the slope with the coefficient value of 5.709 and 3.635 respectively.

Table 2
LR coefficients of landslide causal factors indicating the relative significance for landslide occurrence

Causal factor	Estimate	Signif.	Causal factor	Estimate	Signif.
(Intercept)	-1.282		Needle leaved closed forest	0.633	
Curvature	0.149		Needle leaved open forest	0.780	
Elevation	-6.766	***	Broad leaved closed forest	0.641	
Fault Distance	5.709	***	Broad leaved open forest	0.257	
PGA	0.254		Shrubland	0.337	
Distance to river	0.139		Grassland	-0.269	
Slope	3.635	***	Agriculture	-0.724	
Aspect (< 45)	0.687	*	Bare area	-13.000	
Aspect (45–90)	0.720	**	Sermanthang Formation	-1.250	***
Aspect (90–135)	0.992	***	Simpani Formation	-1.271	***
Aspect (135–180)	0.585	*	Hadikhola Schist	-2.228	***
Aspect (180–225)	1.029	***	Dhadkhola Gneiss	-1.169	***
Aspect (225–270)	1.123	***	Gyalthung Quartzite	-1.497	***
Aspect (270–315)	1.178	***	Pangang Formation	0.000	
Aspect (315–360)	0.353				
Note: Significance in p-value 0.0001 '***', p-value 0.001 '**', p-value 0.01 '*'					

Even though many of these landslides would not occur any time soon without the earthquake shaking, we found that PGA (= 0.254) have a nominal association (statistically) for landslide occurrence in the study area.

The probability values were ranges from 0.001 to 0.975. The final susceptibility map with susceptibility categories- very low, low, medium, high, and very high-are presented in Fig. 6. The area coverage according to the susceptibility categories are 27.75% (101.11 km^2), 25.94% (94.53 km^2), 20.06% (73.11 km^2), 15.54% (56.64 km^2), and 10.70% (39.00 km^2), respectively from extremely low to high.

Figure 6 suggests that the land having higher slope gradient with elevation ranges from 2400–3000 m are highly sensitive for an earthquake-induced landslide in future. Similarly, Pangang and Sermanthang formation of higher Himalayan (Pre-Cambrian) geology including schist, quartzite and gneiss lithology are highly susceptible. Last but not least, the area having less population density is highly vulnerable to the landslides due to the earthquake.

Map validation:

The AUC values of the success rate and prediction rate curve were 0.796 and 0.702 respectively (Fig. 7) suggesting acceptable accuracy. The AUC value of success rate curve suggests that the approach have the capability of 79.6% to classify landslide susceptibility of the study area as well as there exists a good correlation between dependent (landslide occurrences) and independent (causal factors) variables. The AUC values of the prediction rate curve represent that LSM approaches able to predict the future landslides by 70.2%.

The SCAI values are decreasing from very low to very high susceptibility classes (Table 3). The SCAI values for high susceptibility classes are very low (< 1). However, it is higher for extremely low class suggesting the mapping approach produce a susceptible map with satisfactory accuracy.

Table 3
Distribution of landslides and SCAI in the susceptible categories

SN	Susceptibility	% area of category	% of LS in category	SCAI
1	Extremely Low	27.75	4.50	6.172
2	Very Low	25.94	12.32	2.105
3	Low	20.06	20.25	0.991
4	Medium	15.54	30.85	0.504
5	High	10.70	32.08	0.334

Discussion

Selection of training and validation landslide considering the temporal distribution of landslide as in the study of Remondo et al., (2003), and Ayalew and Yamagishi (2005) is appropriate approaches but is challenging to implement (Brabb, 1984; Remondo et al., 2003). However, in this study, we selected the training and validation landslide considering the riverbank because the landslide caused by seismicity occurred at the same time throughout the area.

Landslide susceptibility differs from quake to quake (Kargel et al., 2016). This study concurred with the study of Garcia-Rodriguez et al. (2008) that the landslide density is increasing with the slope gradient. Likewise, the recent study by Kargel et al., (2016) of Nepal found that the earthquake frequencies are higher in the area where slope gradient is more than 30^0 which is similar to our study. However, our study contradicts the study from Kamp et al. (2008) as they found that the landslide relative density is higher in slope 25–35^0 and decrease on either side. Similarly, the study from Roback et al., (2018) also did not found any correlation between landslide occurrences and steepest slopes. Different surficial geology, mostly dominated by a rocky hill which is brittle and more susceptible for shaking, and land cover in the steepest slope gradient might play an essential role for increasing landslide distribution in steeper slope

in this study. This study also concurs with the study of Garcia-Rodrigeuz et al. (2008) that landslide distribution is low at the lower elevation because of the gentle terrain. Similarly, our study found a analogous result with Kamp et al. (2008) that southeast, south and southwest aspect have higher landslides distribution.

As Xu et al. (2015) suggested in their study that only seismogenic faults affect a co-seismic landslide, this study also found the similar result that there is no clear correlation between the distance to the fault line and landslide distribution. The distribution of landslides is random without considering the physical properties of the fault. However, landslide frequencies are increased as the distance from faults line decrease (Xu et al., 2015) because the rock strength weakens due to the fault line (Osmundsen et al., 2009).

We found that the types of metamorphic rock including schist, quartzite, and gneiss found in Pangang formation of the higher Himalayan zone have a higher frequency of landslides which is harmonize with the study by Kargel et al. (2016). The schist of the higher Himalayan zone along with Proterozoic phyllite, amphibolite, meta-sandstone of lesser Himalaya has higher landslide frequency due to the Gorkha earthquake (Kargel et al., 2016). In general, soft sediment (metamorphic rock) usually amplifies the energy of seismic waves (Chamlagain and Gautam, 2015) and amplifies frequencies of the landslide.

The landslide abundance is positively correlated with the seismic intensity (Xu et al., 2015) and is considered as the important for landslide occurrence due to the earthquake (Wang et al., 2003; Xu et al., 2014). However, as in the study by Xu et al. (2015) and Roback et al. (2018), our study found that there is no correlation between the PGA and landslide distribution in the study area. The landslide frequencies in this study area are higher in lower PGA (20%) as in the study by Roback et al. (2018). The excessive slope and increased terrain roughness along the region with lower PGA values (< 20%) in this study area could be the reason for such.

Regarding the association of land cover classes and landslide, this study contrasts the wide-held notion of vegetative area anchors the soil and found to be less susceptible to landslides than agricultural and open area as suggested by the study of Meusburger and Alewell (2008). We found that the forested area has a higher frequency of landslide which is contrasting with the result of the study by Kamp et al. (2008) as they found that grassland and agricultural land have higher earthquake-triggered landslide densities than forest land. The reason for this contrasting result might be dependent with slope distribution as the forested area have higher slope.

In LR analysis, the highest coefficient describes the best predictor which depends upon the trends of the landslide distribution within the classes of each causal factor (Mancini et al., 2010). If there are definite trends as in the causal factors: distance to the fault and slope of this study; their coefficient is positive and higher, which show the positive correlation for landslide occurrences as suggested by the study from Abedini et al. (2017) and vice versa. We found that distance to the fault was the best predictor among the causal factors which contrast the result of Xu et al. (2013): they found the distance from the fault has a negative association for landslide occurrences. It is also believed that landslide frequency often

decreases with increasing distance to the fault (Xu et al., 2015), however, in this study, there is no clear correlation. Various researcher found different factors as the best predictor in their studies such as slope (Ohlmacher and Davis, 2003; Lee and Pradhan, 2007; Yilmaz, 2009; Xu et al., 2013a; Abedini et al., 2017); land cover (Mancini et al., 2010); distance to road (Ayalew and Yamagishi, 2005); terrain roughness and lithology (Garcia-Rodriguez et al., 2008); aspect (Aditian et al., 2018). In the study of Bai et al. (2010), curvature was the best predictor. However, we found that curvature is the less essential factor. Similarly, we found the correlation of PGA in landslide occurrence is weaker compared to other causal factor; even though, the seismic intensity is the reason for land sliding in the region. The triggering factor (either rainfall or earthquake) for landslides (Garcia-Rodriguez et al., 2008) and selection of causal factors could be the reason for such variance in results.

The appearance of the validation landslides in the high susceptibility category determined the performance of the LSM approach which differs among the researcher. Choice of the independent variables (causal factors) (Pradhan and Lee, 2010); mapping approaches used (Nefeslioglu et al., 2008); and local factors as well as the method of selecting training and validation landslides (Xu et al. 2012) could result in the varying accuracy of validation in LSM study. The map validation result of SCAI-decreasing from very low susceptible to very high susceptible categories concurs with the study from Kincal et al. (2009), Sdao et al. (2013), Chen et al. (2016), Abedini et al. (2017), and Nicu and Asandulesei (2018). The prediction AUC value of 70.2% in this study suggest that the LR approach predict the future landslides with satisfactory accuracy despite we use landslides from different regions to train the LSM approach and validate respectively.

Concluding Remarks

Since the susceptibility mapping is the critical aspect for hazard mitigation, we conducted the LSM of the Upper Indrawati watershed of central Nepal, one of the earthquakes affected area due to Gorkha earthquake of M_w 7.8 and its aftershock. In addition to the LSM, we conducted landslide distribution analysis according to the classes of nine causal factors.

The study provided the insight that the landslide occurrences does not show the apparent correlation between the causal factors except slope. Slope angle showed positive correlation for landslide occurrences in the study area as landslide abundance increased with slope angle. The causal factors except elevation and geological formation showed some trends for landslide occurrences resulting in the positive coefficient in LR analysis reaching 5.709 for causal factor 'distance to the fault'. From the study, the region belongs to elevation range (2400-3600) m, distance to the fault (6-9) km, and forested area are highly susceptible to landslides due to the earthquake. Most part of such region belongs to the northern part of the study area where lithology of Pangang formation is dominant and have relatively lower population density.

The multivariate statistical approach, LR, was used for LSM in the study area. The procedure showed the acceptable accuracy with AUC value for success and prediction rate curve of 0.796 and 0.702

respectively, and SCAI values higher in very low category and is descending towards very high vulnerable category. Hence, the map could be used for the slope improvement and generalized planning of the study area. As the rehabilitation and development of the area is ongoing, this map could be an asset for the managers including government and private sectors. Site-specific consideration of local factors needs to be addressed before implementation.

Abbreviations

ANN Artificial Neural Network

AUC Area Under Curve

DEM Digital Elevation Model

FRV Frequency Ratio Value

GIS Geographic Information System

GLM Generalized Linear Model

LAA Landslide Area Abundance

LNA Landslide Number Abundance

LR Logistic Regression

LRD Landslide relative density

LSM Landslide Susceptibility Mapping

PGA Peak Ground Acceleration

SCAI Seed Cell Area Index

SVM Support Vector Machine

Declarations

Availability of data and material

Data will be provided upon request.

Competing interests

The authors declare that they have no competing interest.

Funding

This work is partially supported by Asian Development Bank (ADB)-Japanese Scholarship Program and Kyushu University.

Author's contributions

All authors have contributed for this paper. PG lead the development of this manuscript from study design, data collection and writing. AA contribute for reviewing the manuscript and provide essential feedbacks. TK supervise the study and manuscript development.

Acknowledgement

The study would not be possible without valuable suggestions and inputs from Dr. Andang Soma Suriyana, Dr. Prem Prasad Paudel and Mr. Lok Mani Sapkota. The authors also would like to thank anonymous reviewers for the constructive comments for the improvement of this manuscript.

References

1. Abedini M, Ghasemyan B, Mogaddam MR (2017) Landslide susceptibility mapping in Bijar city, Kurdistan Province, Iran: a comparative study by logistic regression and AHP models. Environ Earth Sci 76(8):308
2. Aditian A, Kubota T, Shinohara Y (2018) Comparison of GIS-based landslide susceptibility models using frequency ratio, logistic regression, and artificial neural network in a tertiary region of Ambon. Indonesia Geomorphology 318:101–111
3. Atkinson PM, Massari R (1998) Generalized linear modeling of susceptibility to landsliding in the Central Apennines, Italy. Comput Geosci 24(4):373–385
4. Ayalew L, Yamagishi H (2005) The application of GIS-based logistic regression for landslide susceptibility mapping in the Kakuda-Yahiko Mountains, Central Japan. Geomorphology 65(1):15–31
5. Ba Q, Chen Y, Deng S, Yang J, Li H (2018) A comparison of slope units and grid cells as mapping units for landslide susceptibility assessment. Earth Sci Inf 11(3):373–388
6. Bai SB, Wang J, Lü GN, Zhou PG, Hou SS, Xu SN (2010) GIS-based logistic regression for landslide susceptibility mapping of the Zhongxian segment in the Three Gorges area, China. Geomorphology 115(1):23–31
7. Brabb EE (1984) Innovative approaches to landslide hazard and risk mapping. Publisher not identified
8. Budimir MEA, Atkinson PM, Lewis HG (2015) A systematic review of landslide probability mapping using logistic regression. Landslides 12(3):419–436

9. Bui DT, Pradhan B, Lofman O, Revhaug I, Dick OB (2012) Landslide susceptibility assessment in the Hoa Binh province of Vietnam: a comparison of the Levenberg–Marquardt and Bayesian regularized neural networks. Geomorphology 171:12–29
10. Chamlagain D, Gautam D (2015) Seismic hazard in the Himalayan intermontane basins: an example from Kathmandu Valley, Nepal. In: Mountain hazards and disaster risk reduction. Springer, Tokyo, pp 73–103
11. Chen W, Li W, Chai H, Hou E, Li X, Ding X (2016) GIS-based landslide susceptibility mapping using analytical hierarchy process (AHP) and certainty factor (CF) models for the Baozhong region of Baoji City, China. Environ Earth Sci 75(1):63
12. Chung CJF, Fabbri AG (2003) Validation of spatial prediction models for landslide hazard mapping. Nat Hazards 30(3):451–472
13. Collins BD, Jibson RW (2015) Assessment of existing and potential landslide hazards resulting from the April 25, 2015 Gorkha, Nepal earthquake sequence (No. 2015 – 1142). US Geological Survey
14. Corominas J, van Westen C, Frattini P, Cascini L, Malet JP, Fotopoulou S, Catani F, Van Den Eeckhaut M, Mavrouli O, Agliardi F, Pitilakis K (2014) Recommendations for the quantitative analysis of landslide risk. Bulletin of engineering geology the environment 73(2):209–263
15. Dai FC, Lee CF (2002) Landslide characteristics and slope instability modeling using GIS, Lantau Island, Hong Kong. Geomorphology 42(3):213–228
16. Dai FC, Lee CF (2003) A spatiotemporal probabilistic modeling of storm-induced shallow landsliding using aerial photographs and logistic regression. Earth surface processes landforms 28(5):527–545
17. Dai FC, Xu C, Yao X, Xu L, Tu XB, Gong QM (2011) Spatial distribution of landslides triggered by the 2008 Ms 8.0 Wenchuan earthquake, China. J Asian Earth Sci 40(4):883–895
18. Delgado J, Garrido J, López-Casado C, Martino S, Peláez JA (2011) On far field occurrence of seismically induced landslides. Eng Geol 123(3):204–213
19. Duncan JM, Wright SG, Brandon TL (2014) Soil strength and slope stability. John Wiley & Sons
20. Fell R, Corominas J, Bonnard C, Cascini L, Leroi E, Savage WZ (2008) Guidelines for landslide susceptibility, hazard and risk zoning for land-use planning. Eng Geol 102(3):99–111
21. Gallen SF, Clark MK, Godt JW, Roback K, Niemi NA (2017) Application and evaluation of a rapid response earthquake-triggered landslide model to the 25 April 2015 Mw 7.8 Gorkha earthquake. Nepal Tectonophysics 714:173–187
22. García-Rodríguez MJ, Malpica JA, Benito B, Díaz M (2008) Susceptibility assessment of earthquake-triggered landslides in El Salvador using logistic regression. Geomorphology 95(3):172–191
23. Goda K, Kiyota T, Pokhrel RM, Chiaro G, Katagiri T, Sharma K, Wilkinson S (2015) The 2015 Gorkha Nepal earthquake: insights from earthquake damage survey. Frontiers in Built Environment 1:8
24. Harp EL, Keefer DK, Sato HP, Yagi H (2011) Landslide inventories: the essential part of seismic landslide hazard analyses. Eng Geol 122(1):9–21

25. Hasegawa S, Dahal RK, Nishimura T, Nonomura A, Yamanaka M (2009) DEM-based analysis of earthquake-induced shallow landslide susceptibility. Geotech Geol Eng 27(3):419–430
26. Hosmer DW, Lemeshow S (2000) Applied Logistic Regression. John Wiley & Sons, New York
27. Huang Y, Zhao L (2018) Review on landslide susceptibility mapping using support vector machines. Catena 165:520–529
28. Kamp U, Growley BJ, Khattak GA, Owen LA (2008) GIS-based landslide susceptibility mapping for the 2005 Kashmir earthquake region. Geomorphology 101(4):631–642
29. Kargel JS, Leonard GJ, Shugar DH, Haritashya UK, Bevington A, Fielding EJ, Fujita K, Geertsema M, Miles ES, Steiner J, Anderson E (2016) Geomorphic and geologic controls of geohazards induced by Nepal's 2015 Gorkha earthquake. Science 351:6269
30. Keefer DK (1994) The importance of earthquake-induced landslides to long-term slope erosion and slope-failure hazards in seismically active regions. In Geomorphology and Natural Hazards (pp. 265–284)
31. Keefer DK (2000) Statistical analysis of an earthquake-induced landslide distribution—the 1989 Loma Prieta, California event. Eng Geol 58(3–4):231–249
32. Keefer DK (2002) Investigating landslides caused by earthquakes–a historical review. Surveys in geophysics 23(6):473–510
33. Kincal C, Akgun A, Koca MY (2009) Landslide susceptibility assessment in the Izmir (West Anatolia, Turkey) city center and its near vicinity by the logistic regression method. Environ Earth Sci 59(4):745–756
34. Kouli M, Loupasakis C, Soupios P, Vallianatos F (2010) Landslide hazard zonation in high risk areas of Rethymno Prefecture, Crete Island. Greece Natural hazards 52(3):599–621
35. Lee S, Pradhan B (2007) Landslide hazard mapping at Selangor, Malaysia using frequency ratio and logistic regression models. Landslides 4(1):33–41
36. Li G, West AJ, Densmore AL, Jin Z, Parker RN, Hilton RG (2014) Seismic mountain building: Landslides associated with the 2008 Wenchuan earthquake in the context of a generalized model for earthquake volume balance. Geochem Geophys Geosyst 15(4):833–844
37. Magliulo P, Di Lisio A, Russo F, Zelano A (2008) Geomorphology and landslide susceptibility assessment using GIS and bivariate statistics: a case study in southern Italy. Nat Hazards 47(3):411–435
38. Mancini F, Ceppi C, Ritrovato G (2010) GIS and statistical analysis for landslide susceptibility mapping in the Daunia area, Italy. Nat Hazards Earth Syst Sci 10(9):1851–1864
39. Marc O, Hovius N, Meunier P, Gorum T, Uchida T (2016) A seismologically consistent expression for the total area and volume of earthquake-triggered landsliding. Journal of Geophysical Research: Earth Surface 121(4):640–663
40. Marzorati S, Luzi L, De Amicis M (2002) Rock falls induced by earthquakes: a statistical approach. Soil Dyn Earthq Eng 22(7):565–577

41. Meusburger K, Alewell C (2008) Impacts of anthropogenic and environmental factors on the occurrence of shallow landslides in an alpine catchment (Urseren Valley, Switzerland). Nat Hazards Earth Syst Sci 8:509–520
42. Montgomery DR, Schmidt KM, Greenberg HM, Dietrich WE (2000) Forest clearing and regional landsliding. Geology 28(4):311–314
43. Nandi A, Shakoor A (2010) A GIS-based landslide susceptibility evaluation using bivariate and multivariate statistical analyses. Eng Geol 110(1):11–20
44. Nefeslioglu HA, Gokceoglu C, Sonmez H (2008) An assessment on the use of logistic regression and artificial neural networks with different sampling strategies for the preparation of landslide susceptibility maps. Eng Geol 97(3):171–191
45. Nicu IC, Asăndulesei A (2018) GIS-based evaluation of diagnostic areas in landslide susceptibility analysis of Bahluieț River Basin (Moldavian Plateau, NE Romania). Are Neolithic sites in danger? Geomorphology 314:27–41
46. Nowicki MA, Wald DJ, Hamburger MW, Hearne M, Thompson EM (2014) Development of a globally applicable model for near real-time prediction of seismically induced landslides. Engineering geology 173:54–65
47. Ohlmacher GC, Davis JC (2003) Using multiple logistic regression and GIS technology to predict landslide hazard in northeast Kansas. USA Engineering Geology 69(3):331–343
48. Osmundsen PT, Henderson I, Lauknes TR, Larsen Y, Redfield TF, Dehls J (2009) Active normal fault control on landscape and rock-slope failure in northern Norway. Geology 37(2):135–138
49. Owen LA, Kamp U, Khattak GA, Harp EL, Keefer DK, Bauer MA (2008) Landslides triggered by the 8 October 2005 Kashmir earthquake. Geomorphology 94(1):1–9
50. Parameswaran RM, Natarajan T, Rajendran K, Rajendran CP, Mallick R, Wood M, Lekhak HC (2015) Seismotectonics of the April–May 2015 Nepal earthquakes: An assessment based on the aftershock patterns, surface effects and deformational characteristics. J Asian Earth Sci 111:161–174
51. Pourghasemi HR, Rahmati O (2018) Prediction of the landslide susceptibility: Which algorithm, which precision? Catena, 162, 177–192
52. Pradhan B, Lee S (2010) Landslide susceptibility assessment and factor effect analysis: backpropagation artificial neural networks and their comparison with frequency ratio and bivariate logistic regression modelling. Environ Model Softw 25(6):747–759
53. Remondo J, González A, De Terán JRD, Cendrero A, Fabbri A, Chung CJF (2003) Validation of landslide susceptibility maps; examples and applications from a case study in Northern Spain. Nat Hazards 30(3):437–449
54. Roback K, Clark MK, West AJ, Zekkos D, Li G, Gallen SF, Chamlagain D, Godt JW (2018) The size, distribution, and mobility of landslides caused by the 2015 Mw7. 8 Gorkha earthquake. Nepal Geomorphology 301:121–138
55. Robinson TR, Rosser NJ, Densmore AL, Williams JG, Kincey ME, Benjamin J, Bell HJ (2017) Rapid post-earthquake modelling of coseismic landslide magnitude and distribution for emergency

response decision support. Natural hazards earth system sciences discussions 17:1521–1540

56. Robinson TR, Davies TRH (2013) Potential geomorphic consequences of a future great (Mw = 8.0+) Alpine Fault earthquake, South Island, New Zealand. Natural hazards earth system sciences 13(9):2279–2299
57. Sdao F, Lioi DS, Pascale S, Caniani D, Mancini IM (2013) Landslide susceptibility assessment by using a neuro-fuzzy model: a case study in the Rupestrian heritage rich area of Matera. Natural hazards earth system sciences 13(2):395–407
58. Suzen ML, Doyuran V (2004) A comparison of the GIS based landslide susceptibility assessment methods: multivariate versus bivariate. Environmental geology 45(5):665–679
59. Suzen ML, Kaya BS (2012) Evaluation of environmental parameters in logistic regression models for landslide susceptibility mapping. Int J Digit Earth 5(4):338–355
60. Van Westen CJ, Seijmonsbergen AC, Mantovani F (1999) Comparing landslide hazard maps. Natural hazards 20(2–3):137–158
61. Varnes DJ (1978) Slope movement types and processes. Transportation Research Board Special Report, (176)
62. Xu C, Xu X (2012) Comment on “Spatial distribution analysis of landslides triggered by 2008.5. 12 Wenchuan Earthquake, China” by Shengwen Qi, Xu Q, Lan H, Zhang B, Jianyou Liu [Engineering Geology 116 (2010) 95–108]. Engineering Geology, 133, 40–42
63. Xu C, Xu X, Shyu JBH (2015) Database and spatial distribution of landslides triggered by the Lushan, China Mw 6.6 earthquake of 20 April 2013. Geomorphology 248:77–92
64. Xu C, Xu X, Dai F, Saraf AK (2012) Comparison of different models for susceptibility mapping of earthquake triggered landslides related with the 2008 Wenchuan earthquake in China. Comput Geosci 46:317–329
65. Xu C, Xu X, Dai F, Wu Z, He H, Shi F, Wu X, Xu S (2013a) Application of an incomplete landslide inventory, logistic regression model and its validation for landslide susceptibility mapping related to the May 12, 2008 Wenchuan earthquake of China. Natural hazards 68(2):883–900
66. Xu C, Xu X, Yao Q, Wang Y (2013b) GIS-based bivariate statistical modelling for earthquake-triggered landslides susceptibility mapping related to the 2008 Wenchuan earthquake, China. Quarterly journal of engineering geology hydrogeology 46(2):221–236
67. Xu C, Xu X, Yao X, Dai F (2014) Three (nearly) complete inventories of landslides triggered by the May 12, 2008 Wenchuan Mw 7.9 earthquake of China and their spatial distribution statistical analysis. Landslides 11(3):441–461
68. Yalcin A, Bulut F (2007) Landslide susceptibility mapping using GIS and digital photogrammetric techniques: a case study from Ardesen (NE-Turkey). Natural hazards 41(1):201–226
69. Yao X, Tham LG, Dai FC (2008) Landslide susceptibility mapping based on support vector machine: a case study on natural slopes of Hong Kong, China. Geomorphology 101(4):572–582

70. Yilmaz I (2009) Landslide susceptibility mapping using frequency ratio, logistic regression, artificial neural networks and their comparison: a case study from Kat landslides (Tokat—Turkey). Comput Geosci 35(6):1125–1138
71. Zhou G, Esaki T, Mitani Y, Xie M, Mori J (2003) Spatial probabilistic modeling of slope failure using an integrated GIS Monte Carlo simulation approach. Eng Geol 68(3):373–386

Figures

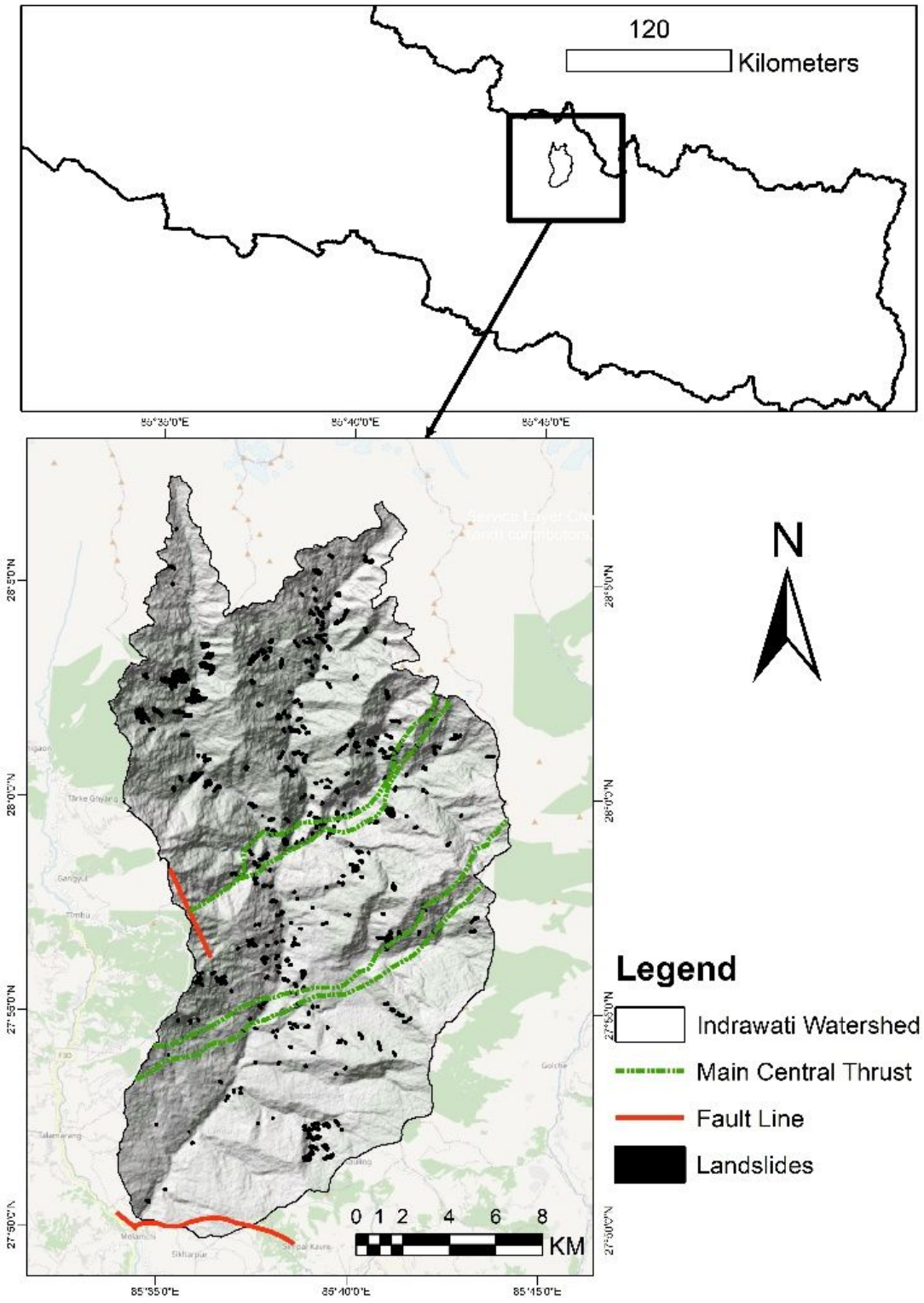

Figure 1

Study area location on the map of Nepal. MCT and fault line was also shown Note: The designations employed and the presentation of the material on this map do not imply the expression of any opinion whatsoever on the part of Research Square concerning the legal status of any country, territory, city or area or of its authorities, or concerning the delimitation of its frontiers or boundaries. This map has been provided by the authors.

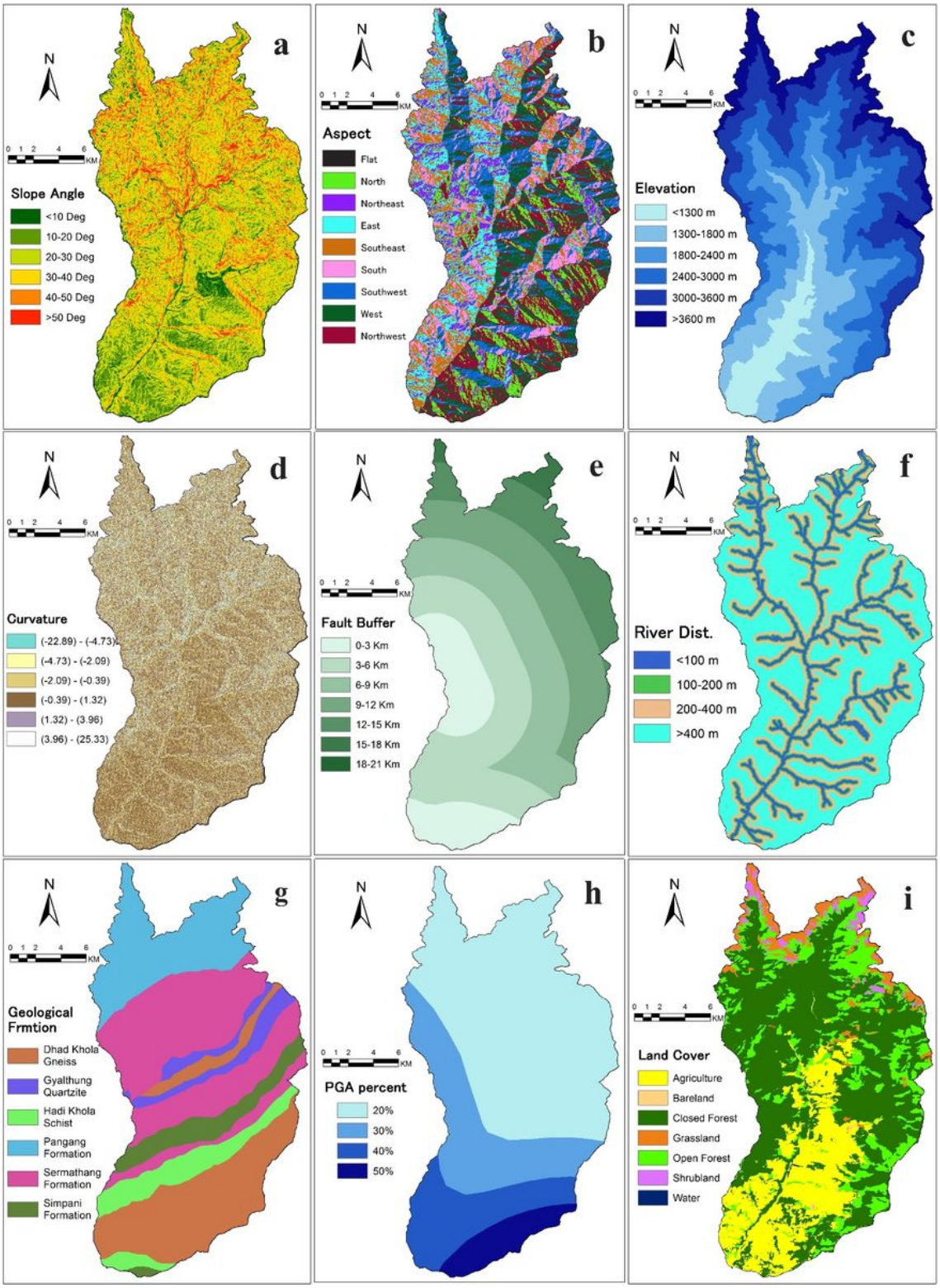

Figure 2

Categorized landslide causative factor's map of the study area (a) slope angle, (b) aspect, (c) elevation, (d) curvature, (e) distance to the fault, (f) distance to the river, (g) geological formation, (h) seismic intensity, and (i) land cover Note: The designations employed and the presentation of the material on this map do not imply the expression of any opinion whatsoever on the part of Research Square concerning

the legal status of any country, territory, city or area or of its authorities, or concerning the delimitation of its frontiers or boundaries. This map has been provided by the authors.

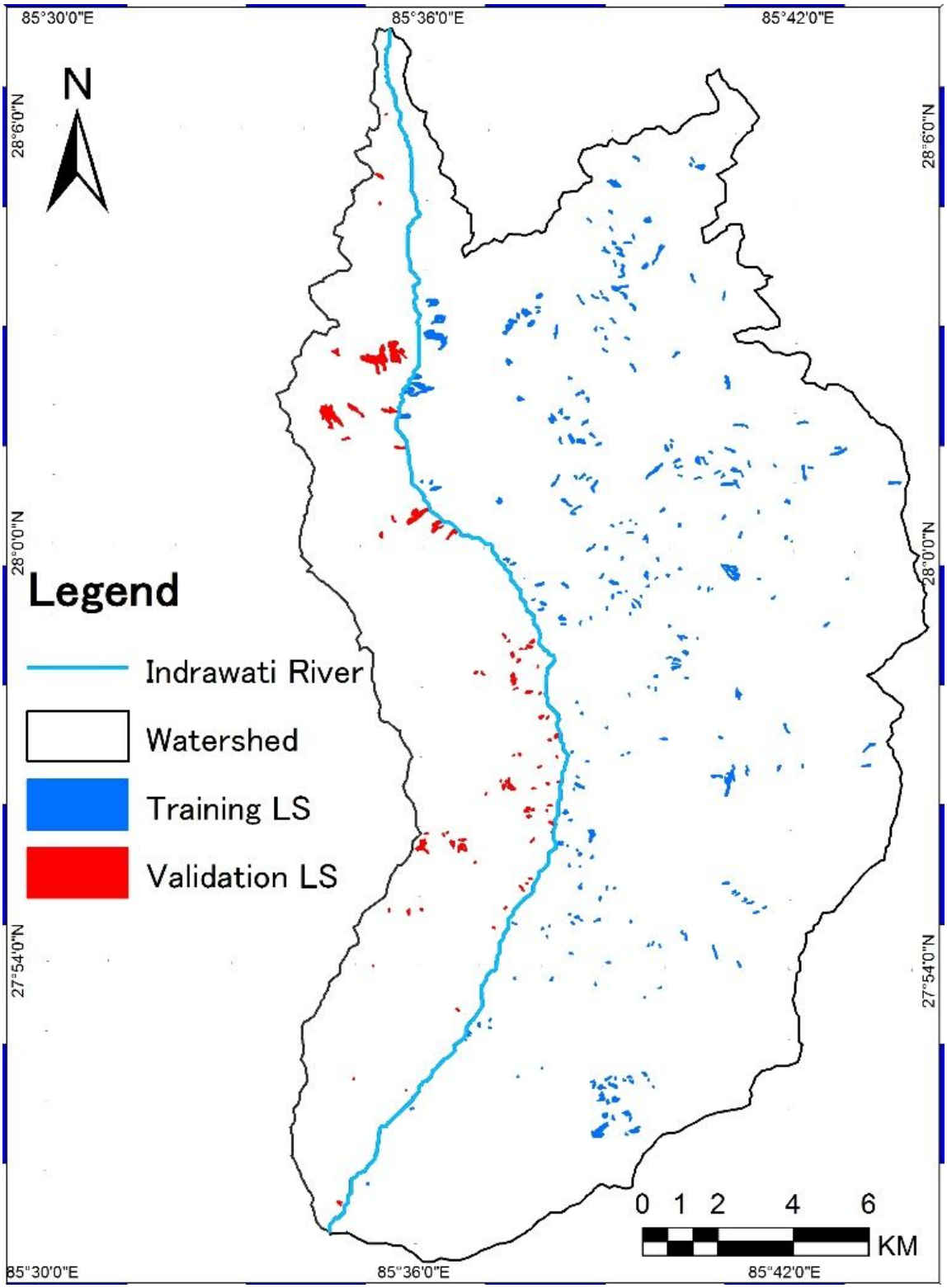

Figure 3

Distribution of training landslides (landslides in the left bank of Indrawati River) and validation landslides (landslides in the right bank of Indrawati River). Indrawati River was also shown in the map which flows from North to South Note: The designations employed and the presentation of the material on this map

do not imply the expression of any opinion whatsoever on the part of Research Square concerning the legal status of any country, territory, city or area or of its authorities, or concerning the delimitation of its frontiers or boundaries. This map has been provided by the authors.

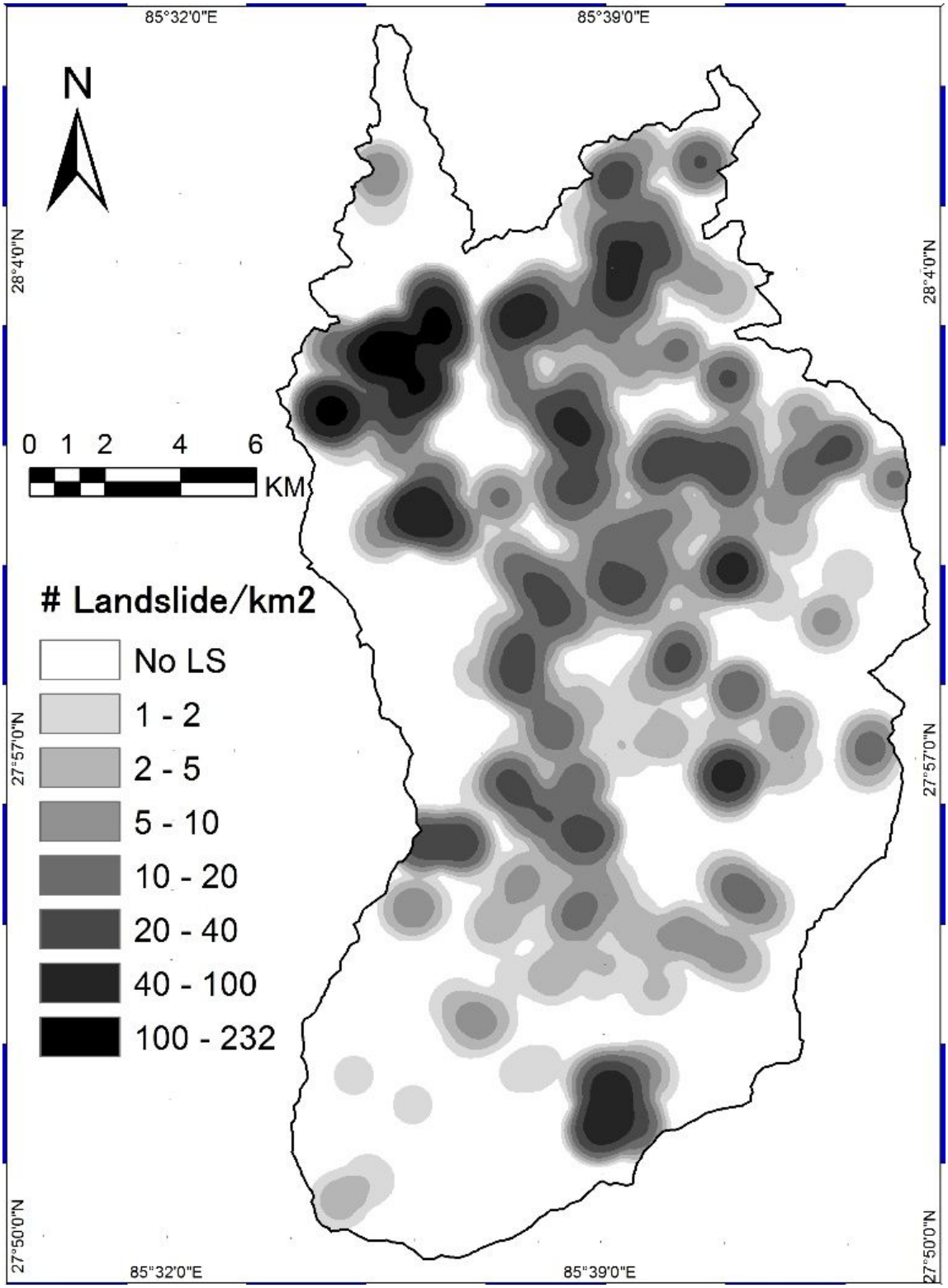

Figure 4

Landslide density (# of landslide per km2) of the study area due to the Gorkha earthquake of 2015 Note: The designations employed and the presentation of the material on this map do not imply the expression

of any opinion whatsoever on the part of Research Square concerning the legal status of any country, territory, city or area or of its authorities, or concerning the delimitation of its frontiers or boundaries. This map has been provided by the authors.

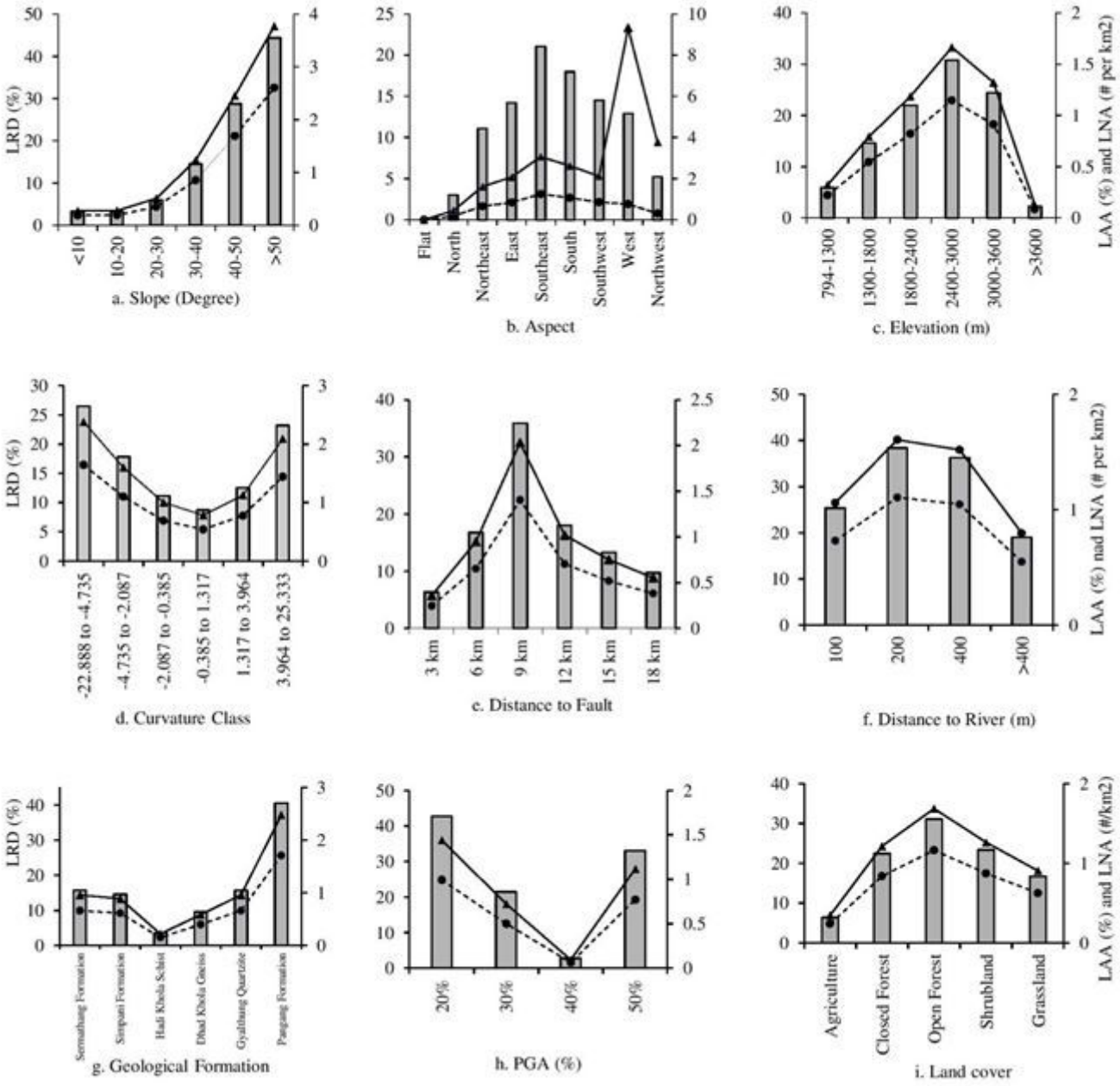

Figure 5

Landslide distribution according to the classes of causal factors (a. slope, b. aspect, c. elevation, d. curvature, e. distance to the fault, f. distance to the river, g. geological formation, h. peak ground acceleration, and i. land cover). The bar graph represents the LRD in percent shown in the primary y-axis. The dotted line with round marker represents LAA (%), and line with triangular marker represents LNA (landslide #/km2); depicted in the secondary y-axis

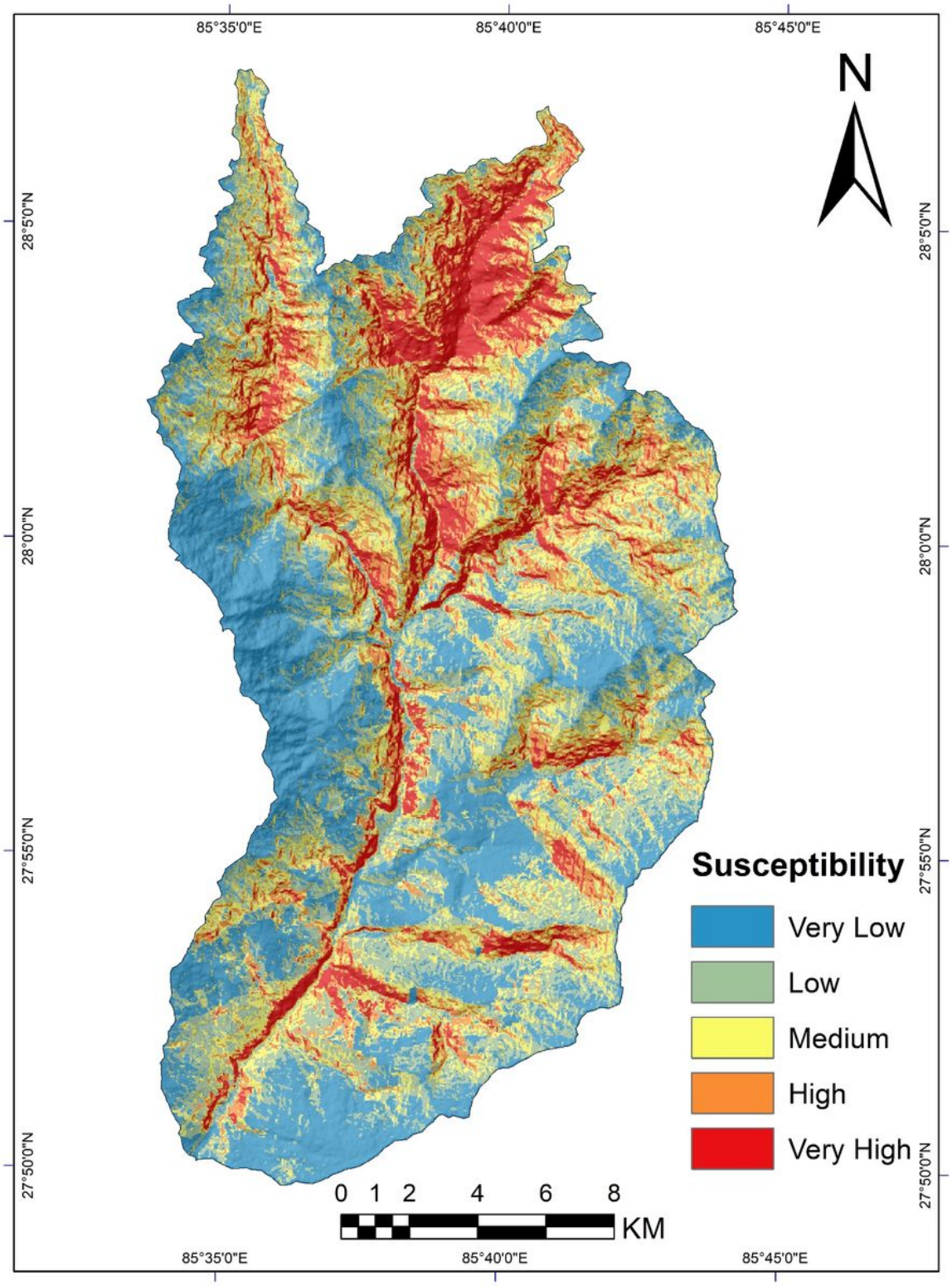

Figure 6

Simplified map of landslide susceptibility due to earthquake depicting the susceptibility classes of the study area Note: The designations employed and the presentation of the material on this map do not imply the expression of any opinion whatsoever on the part of Research Square concerning the legal status of any country, territory, city or area or of its authorities, or concerning the delimitation of its frontiers or boundaries. This map has been provided by the authors.

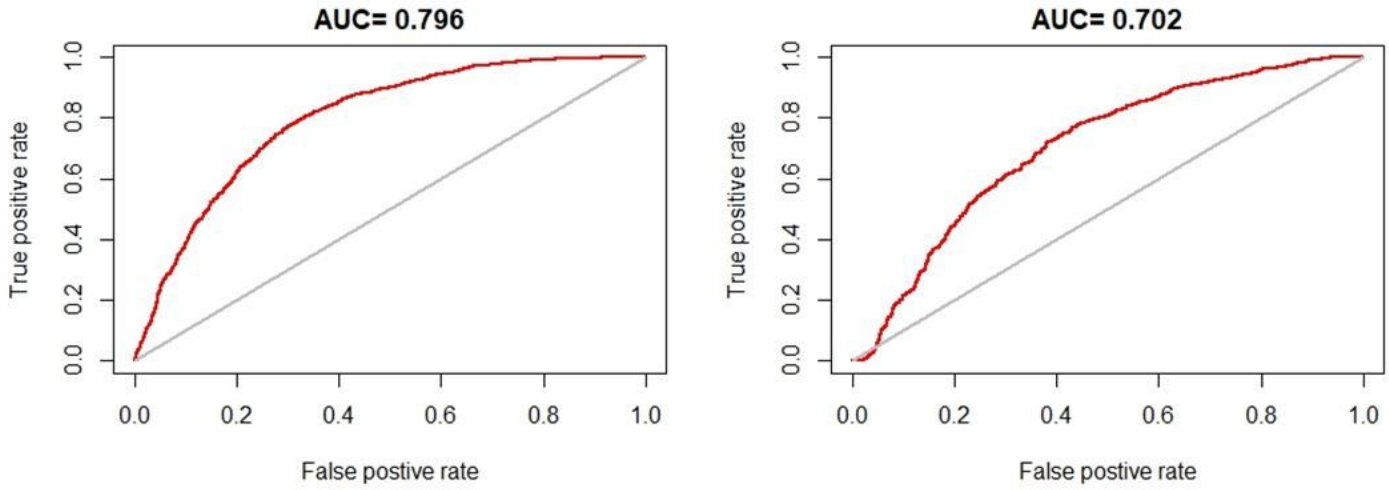

Figure 7

AUC values representing the accuracy of the LSM approach (left) success rate curve, and (right) prediction rate curve